Soft Matter

Boundary Layer Description of Directional Polymer Crystallisation

Journal:	*Soft Matter*
Manuscript ID	SM-ART-06-2021-000913.R1
Article Type:	Paper
Date Submitted by the Author:	26-Jul-2021
Complete List of Authors:	Adhikari, Sabin; Columbia University, Chemical Engineering Krauskopf, Alejandro; Columbia University, Chemical Engineering Kumar, Sanat; Columbia University, Thampi, Sumesh; Indian Institute of Technology Madras, Chemical Engineering Durning, Chris; Columbia University, Chemical Engineering

SCHOLARONE™
Manuscripts

Soft Matter

Boundary Layer Description of Directional Polymer Crystallisation

Sabin Adhikari,[a] Alejandro A. Krauskopf,[a] Sanat K. Kumar,[*a] Sumesh P. Thampi,[*b] Christopher J. Durning[a]

Nearly fifty years ago Lovinger and Gryte suggested that the directional crystallization of a polymer was analogous to the quiescent isothermal crystallization experiment but at a supercooling where the crystal growth velocity was equal to the velocity of the moving front. Our experiments showed that this equivalence holds in a detailed manner at low directional velocities. To understand the underlying physics of these situations, we modeled the motion of a crystallization front in a liquid where the left side boundary is suddenly lowered below the melting point (Stefan's problem) but with the modification that the crystallization kinetics follow a version of the Avrami model. Our numerical results surprisingly showed that the results of the polymer analog track with the Stefan results which were derived for a simple liquid that crystallizes completely at its melting point; in particular, the position of the crystal growth-front evolved with time exactly as in the Stefan problem. The numerical solution also showed that the temperature in the immediate vicinity of the growth-front decreased with increasing front velocity, which is in line with Lovinger and Gryte's ansatz. To provide a clear theoretical understanding of these numerical results we derive a boundary layer solution to the governing coupled differential equations of the polymer problem. The analytical results are in agreement with our observations from experiments and numerical computations but show that this equivalence between the small molecule and polymer analog only holds in the limit where the crystallization enthalpy is much larger than the rate at which heat is conducted away in the polymer. In particular, in the context of the temperature profile, the enthalpy generated by the crystallisation process which is spread out over a narrow spatial region can be approximated as a point source whose location and temperature correspond to the Lovinger-Gryte ansatz.

1   Introduction

Zone annealing (ZA) is a material processing technique heavily used in the purification of semiconductors[1,2]. The potential use of ZA in polymer processing was explored by Lovinger and Gryte[3–5] in seventies, and has been extended more recently by us[6]. Lovinger and Gryte conjectured that at a steady-state, the velocity at which a crystallising sample is moved through the heat source sets the crystal growth velocity; they further suggested that each ZA experiment, therefore, corresponds to an isothermal crystallisation experiment at a temperature where the crystal growth velocity matches the ZA velocity.

In a recent paper[7], we developed a theoretical framework for modeling ZA for polymer-like materials whose crystal growth kinetics are dependent on temperature. As a first step towards modeling ZA for such materials, we considered the classic Ste-

fan problem with two modifications: unlike in the Stefan problem where the melting occurs at the melting point only, we allowed the material to crystallise at any temperature below the melting temperature by assuming a linear temperature dependence, and we adopted a simple version of the Avrami model for the growth kinetics. The resulting coupled differential equations were solved numerically to find the temperature and the associated crystallinity profiles. The numerical results showed an identical time evolution for the position of the solid-liquid interface to the progress of the solid-liquid interface in the corresponding Stefan problem. In addition, the scale of the steady-state temperature field near the interface was found to relate inversely with the growth-front velocity. While this velocity dependence of the interface temperature is consistent with Lovinger's ansatz that there exists an equivalent isothermal crystallisation temperature for each growth-front speed at steady state, theoretical understanding of above observations, that is, the identical evolution of interface position with Stefan's problem, and the growth-front velocity dependence of interface temperature field is somewhat

[a] Department of Chemical Engineering, Columbia University, New York, New York 10027, United States; E-mail: sk2794@columbia.edu.
[b] Department of Chemical Engineering, Indian Institute of Technology, Madras, 600036, India; E-mail: sumesh@iitm.ac.in
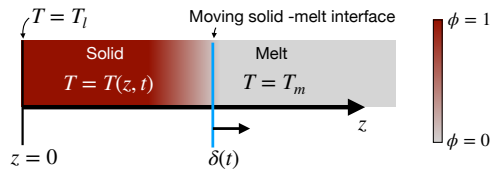
Fig. 1 A schematic of the problem considered in this work. Polymer melt at a temperature of $T = T_m$ is cooled by imposing a lower temperature T_l at $z = 0$. As a consequence melt crystallises and the crystal-melt boundary advances to the right. The color shows the extent of crystallisation, quantified by the volume fraction of the crystals.

limited.

In this study, we consider the same modified Stefan problem and provide an approximate boundary layer solution to the governing differential equations. For a large latent heat and in the limit of long time our analytical results show that the position of the solid-liquid interface tracks the interface position in the Stefan problem. Also, the effective super-cooling for crystallization within the boundary layer varies inversely with the front speed.

The rest of this paper is organized as follows. In section 2, we present a mathematical model for polymer melt crystallisation initially just above its melting point in the one-dimensional thermal field created by a sudden stationary sink at one boundary. After scaling, section 3 delivers an approximate solution by asymptotic methods for the temperature and crystallinity fields for the case of (relatively) large latent heats, appropriate for polymer systems. Comparisons with the Stefan model, and key results supporting the Lovinger-Gryte ansatz are presented. Section 4 compares the analytics with numerical solutions of the governing equations.

2 Modelling polymer melt crystallisation

In this section, we describe the system investigated in this work and formulate the mathematical description of the crystallisation process. As shown in Fig. 1, we consider a one-dimensional domain (z-direction) of a polymer melt, initially maintained at a uniform temperature of $T = T_m$. If the left-hand boundary of the polymer melt is changed to a temperature T_l such that $T_l < T_m$, the polymer melt cools and undergoes crystallisation, a phase change from the melt to a solid phase. The spatial homogeneity of crystallisation process depends upon the particular material under consideration, but the extent of crystallisation increases with time as long as the temperature of the left boundary is maintained at a lower temperature relative to the equilibrium melting temperature. The objective of the present work is to investigate the heat transfer processes in the material during the phase change, and thus to analytically determine the temperature and crystallinity profiles in the material.

2.1 Mathematical formulation

The evolution of temperature is one directional in the material undergoing crystallisation, $T(z,t)$ and is given by the solution of the unsteady heat equation,

$$\frac{\partial T}{\partial t} = \frac{k}{\rho C}\frac{\partial^2 T}{\partial z^2} + \frac{L}{C}\frac{\partial \phi}{\partial t} + Q, \tag{1}$$

where k is the thermal conductivity, ρ is the density and C is the specific heat capacity of the material. The latent heat of crystallisation is denoted by L, the rate of crystallisation by $\frac{\partial \phi}{\partial t}$ and the direct heat exchange of the material with the surroundings is accounted by Q. Here, the local volume fraction of the crystal phase, which is a function of space and time, is denoted by $\phi(z,t)$. Hence, eqn. 1 describes that the temperature $T(z,t)$ is determined by the conductive heat flux, the latent heat released during the crystallisation process and any other loss/gain from the surroundings. In our analysis, without loss of generality, we consider (i) $Q = 0$ and (ii) the melt and the solid phases have the same physical (thermal) properties, namely thermal diffusivity, $k/(\rho C)$ and specific heat capacity, C.

As the polymer melt cools down crystals nucleate and grow locally in the thermal field. The specific mechanism of nucleation and growth may depend upon several aspects of the system, such as the presence of nucleating agents, characteristics of the thermal field imposed, etc. In our modeling we adopt the simplest possible scenario relevant to real systems. To make clear the simplifications adopted in specifying a kinetic equation for the local crystallization kinetics, a brief recap of Avrami's law is presented in appendix A.1.

In one dimension, assuming instantaneous nucleation, the Avrami crystallization kinetics may be written as (see eqns. 55 and 58 in appendix A.1)

$$\frac{d\phi}{dt} = \begin{cases} R(1-\phi)\left(1 - \frac{T}{T_m}\right), & T \leq T_m \\ 0, & T > T_m, \end{cases} \tag{2}$$

where R is a constant of proportionality that describes the rate of crystallisation and T_m is a well-defined melting point for the material. Therefore, crystallisation occurs at any temperature $T < T_m$, allowing the material to undercool. Also the form of the above expression indicates that the material is allowed to have a maximum crystallinity of 1 consistent with the definition of ϕ. Eqn. 2 incorporates the important features of crystallisation kinetics, i.e, the rate of crystallisation increases with an increase in undercooling (the difference in temperature with respect to T_m) and decreases with an increase in the degree of crystallinity. Both these driving forces appear as linear dependences in eqn. 2.

Hence, the temperature profile dictates the crystallisation kinetics in the material while the latent heat released during the crystallisation and the imposed boundary conditions dictate the temperature profile in the material. In other words, in the problem discussed in Fig. 1, a continuous heat flux from the crystallising front to the left hand boundary of the domain prevails. As a result, the crystallising front advances to the right, thus making the whole process unsteady. The coupled evolution of temperature and crystallinity in the material is given by a simultaneous solution of the governing equations: eqn. 1 and eqn. 2.

We define $\delta(t)$ to be the boundary position where T departs from T_m and crystallinity begins to develop. Thus, the phase boundary $\delta(t)$ to be determined as part of the solution using the condition

$$T(z = \delta(t), t) = T_m. \tag{3}$$

If the melt is made up of small molecules which exhibit a sharp melting point, the problem described above reduces to the classical Stefan problem[8]. In this case, an analytical solution is well known: the temperature exhibits a self similar profile while the crystallinity profile has a step change at the crystal-melt boundary. On the other hand, the problem of a crystallising polymer melt is less well-explored. In our earlier study, we solved eqn. 1 and eqn. 2 numerically. Our simulations established that the polymer crystallisation problem closely follows the Stefan solution if the imposed driving force, namely the temperature difference $T_m - T_l$ is relatively small. Hence we investigate the polymer crystallisation problem further and seek an analytical solution in the limit of small driving force, $T_m - T_l$. As illustrated below, this problem exhibits rich phenomenology with a boundary layer structure that allows us to determine an analytical solution to the 'Polymer Stefan problem' in a perturbative fashion. We obtain analytical expressions for the spatio-temporal dependence of both temperature and crystallinity as well as the rate of advancement of the crystallising front. Analysis of the latter quantity also validates the Lovinger–Gryte conjecture that the crystal growth velocity is directly proportional to the extent of undercooling.

2.2 Non-dimensionalisation

To make the problem analytically tractable we introduce the following non-dimensional variables: $\tilde{T} = \frac{T_m - T}{T_m - T_l}$ and $\tilde{\phi} = \phi$. Thus, the rescaled temperature, $\tilde{T} = 0$ in the melt phase and $\tilde{T} = 1$ at the left boundary. The characteristic time scale is based on the rate of crystallisation: $\tilde{t} = (Rt)\frac{T_m - T_l}{T_m}$. Similarly, all lengths can be non-dimensionalised as $\tilde{z} = \frac{z}{d}$ where $d = \sqrt{\frac{k}{R\rho C \frac{T_m - T_l}{T_m}}}$, a characteristic length set by the thermal diffusivity, $k/(\rho C)$ based on the characteristic time scale of crystallisation. Using these non-dimensionalisations, eqns. 1 and 2 reduce to

$$\frac{\partial \tilde{T}}{\partial \tilde{t}} = \frac{\partial^2 \tilde{T}}{\partial \tilde{z}^2} - \frac{1}{\varepsilon}\frac{\partial \tilde{\phi}}{\partial \tilde{t}}, \qquad (4)$$

and

$$\frac{d\tilde{\phi}}{d\tilde{t}} = \begin{cases} (1 - \tilde{\phi})\tilde{T}, & \tilde{T} \geq 0 \\ 0, & \tilde{T} < 0, \end{cases} \qquad (5)$$

respectively. A single non-dimensional number, $\varepsilon = \frac{(T_m - T_l)}{(L/C)}$, the ratio of the imposed driving force for crystallisation, $T_m - T_l$, to the temperature scale set by the latent and specific heat capacity of the material, L/C, arises in the formulation and hence this parameter alone controls the dynamic evolution of temperature and crystallisation in the melt.

If ε were large then eqn. 4 becomes the simple heat conduction equation, which can be solved independent of the crystallization profile; the evolution of crystal fraction then can be obtained from the resulting z and t dependent temperature profile. For typical values of $T_m - T_l \approx$ 10K, and L and C values for polymers yields a $\varepsilon \approx$ 0.1-0.2. Of course large ε values can be obtained for large $T_m - T_l$ but in these regimes, far below the melting point, other phenomena such as the role of the glass transition on crystallization kinetics takes over. This is not of our interest and thus we focus on situations where $\varepsilon \to 0$. In the rest of the text, we drop

the tilde sign ˜ of non-dimensional variables for the simplicity in notation.

3 Boundary layer crystallisation model

3.1 Asymptotic solution

Having recognized that ε is the only non-dimensional parameter that controls the crystallisation process, we seek an approximate analytical solution of eqns. 4-5 in the limit of $\varepsilon << 1$. This limit corresponds to a weak driving force for heat transfer. Assuming a regular perturbation expansion for temperature and crystallinity in the crystallising region of the polymer ($z < \delta(t)$), we assume

$$T(z,t) \sim \mathscr{T}_0(z,t) + \varepsilon \mathscr{T}_1(z,t) + O(\varepsilon^2), \qquad (6)$$

$$\phi(z,t) \sim \Phi_0(z,t) + \varepsilon \Phi_1(z,t) + O(\varepsilon^2). \qquad (7)$$

Substituting in eqns. 4-5 and collecting terms in the order of hierarchy, at $O(\varepsilon^0)$,

$$0 = \frac{\partial}{\partial t}\Phi_0, \qquad (8)$$

$$\frac{\partial}{\partial t}\Phi_0 = (1 - \Phi_0)\mathscr{T}_0, \qquad (9)$$

which suggests $\Phi_0(z,t) = 1$ as a possible solution but that cannot satisfy the auxiliary condition on Φ, namely $\Phi \to 0$ at $z = \delta(t)$. It also leaves the temperature profile $\mathscr{T}_0$ undetermined. Similarly, it could also yields $\mathscr{T}_0 = 0$ at which point $\Phi_0(z,t) = 0$ (i.e., since the crystallisation with take an infinite amount of time). So, this solution captures the two bulk phases without proper modeling the regions where the temperature and crystallanity vary.

3.2 Boundary layer approximation

The solution $(\Phi_0, \mathscr{T}_0)$ discussed above arises because the naive regular perturbation expansion resulted in the disappearance of all derivatives of temperature in eqn. 8 at $O(\varepsilon^0)$. The disappearance of the highest order derivative of temperature in the governing equation and hence the solutions failing to satisfy all boundary conditions is the classical signature of the boundary layer structure of the problem. Physically, we expect crystallisation near the solid-melt boundary ($z = \delta(t)$) to release sufficient heat that the conductive heat transfer (highest order derivative in eqn. 4) in the vicinity of the phase boundary cannot be neglected. Moreover in this region, crystallinity can be expected to show a large change from $\phi = 0$ corresponding to that in the melt to a finite and large ϕ corresponding to crystals in the solid region. Numerical simulations reported in our earlier work[7] are in accordance with these expectations.

Therefore, we propose a boundary layer solution to this problem. To this point, a composite solution needs to be calculated, wherein, to the left of the moving phase boundary $\delta(t)$, there exists a boundary layer, a thin region where crystallinity is low compared to the rest of the solid region ("inner" layer). Outside this boundary layer where crystallinity is comparatively higher is termed as the "outer" layer. Governing equations are to be separately solved in the inner and outer layer while ensuring appro-

priate continuity in the solutions in the two regions.

3.2.1 Solution in the outer layer

We assume the following asymptotic expansions for temperature and crystallinity in terms of the variable ε,

$$T^o(z,t) \sim T_0^o(z,t) + \varepsilon^a T_1^o(z,t) + O(\varepsilon^{2a}) \tag{10}$$

$$\phi^o(z,t) \sim \phi_0^o(z,t) + \varepsilon^b \phi_1^o(z,t) + O(\varepsilon^{2b}). \tag{11}$$

where the superscript 'o' refers to the outer solution, and the subscripts refer to increasing orders in the expansion. The unknown exponents a and b need to be determined. Substituting in eqns. 4-5 and collecting terms in the order of hierarchy, at $O(\varepsilon^0)$,

$$0 = \frac{\partial}{\partial t}\phi_0^o, \tag{12}$$

$$\frac{\partial}{\partial t}\phi_0^o = (1-\phi_0^o)T_0^o. \tag{13}$$

Thus we obtain $\phi_0^o(z,t) = 1$ in the outer layer. Again, at this order, T_0^o is undetermined but it can be calculated by considering terms in the next order in hierarchy. Using $b = 1$ (the value of a does not need to be defined for this analysis) we find that, at $O(\varepsilon^1)$,

$$\frac{\partial}{\partial t}T_0^o = \frac{\partial^2}{\partial z^2}T_0^o - \frac{\partial}{\partial t}\phi_1^o, \tag{14}$$

$$\frac{\partial}{\partial t}\phi_1^o = -\phi_1^o T_0^o. \tag{15}$$

It turns out that $\phi^o(z,t) = 1$ is unequivocally satisfied in the outer layer even at $O(\varepsilon^1)$. This is justified in the analysis done in the next section 3.2.2 where it is shown that the $\phi^o \to 1$ is acceptable condition in the matching region between the outer and the inner layer (i.e, the boundary condition on the right hand edge of the outer layer). In other words, $\phi_1^o = 0$ and there are no corrections at $O(\varepsilon^1)$ to the crystallinity profile, $\phi_0^0 = 1$ in the outer layer. Then the resulting equation for $T_0^o(z,t)$ in the outer layer is the standard heat equation, which exhibits a similarity solution

$$T_0^o(z,t) = 1 - \alpha \operatorname{erf}\left(\frac{z}{2\sqrt{t}}\right). \tag{16}$$

This temperature profile satisfies the boundary condition $T_0^o(z = 0,t) = 1$ on the left hand side of the domain. The constant α has to be determined by matching the temperature profile with the solution in the inner layer. It may be noted that at long times, $t \gg 1$, a pseudo steady solution can be written down instead of eqn. 16. This can be easily seen by analyzing eqn. 14. At long times, when $\frac{\partial}{\partial t}T_0^o \sim \frac{1}{t} \ll 1$, we have, $\frac{\partial^2}{\partial z^2}T_0^o = 0$ and temperature becomes a linear function of z. This is an important new insight that we shall use below.

3.2.2 Solution in the boundary layer

To appropriately non-dimensionalise variables we define a boundary layer coordinate

$$s = \frac{\delta(t)-z}{\varepsilon^c} \; ; \; c > 0. \tag{17}$$

The value of c will be discussed below. Note that the boundary layer exists to the left of the solid-melt phase boundary $\delta(t)$ and hence $s > 0$. Then the governing equations can be transformed to the boundary layer coordinate s (see appendix A.2).

Assuming asymptotic expansions of the following form for temperature and crystallinity in the boundary layer,

$$T^i(s,t) \sim T_0^i(s,t) + \varepsilon^d T_1^i(s,t) + o(\varepsilon^d) \; ; \; d > 0,$$

$$\phi^i(s,t) \sim \phi_0^i(s,t) + \varepsilon^e \phi_1^i(s,t) + o(\varepsilon^e) \; ; \; e > 0.$$

Substituting in the governing equations (eqns. 64-65 in the appendix) and collecting terms at the order of hierarchy, we obtain at $O(\varepsilon^0)$

$$0 = \frac{\partial^2 T_0^i(s,t)}{\partial s^2} - \frac{\partial \phi_0^i(s,t)}{\partial t}, \tag{18}$$

$$\frac{\partial \phi_0^i(s,t)}{\partial t} = (1-\phi_0^i)T_0^i. \tag{19}$$

In eqn. 18, the dominant balance between the conductive heat flux and the heat released via latent heat of crystallisation is achieved by (i) selecting $c = \frac{1}{2}$ in eqn. 17 and (ii) assuming the pseudo-steady state limit for temperature, $t \gg 1$. The latter assumption amounts to restricting the analysis to long times when $d\delta/dt \ll \sqrt{\varepsilon}$. Substituting eqn. 19 in eqn. 18 and eliminating $T_0^i(s,t)$ we obtain

$$\frac{\partial^2}{\partial s^2}\ln(1-\phi_0^i) + \phi_0^i = f(s), \tag{20}$$

where $f(s)$ is a function of s but independent of time (consistent with the asymptotic, psuedo-steady state approximation utilized). This equation is second order in s and it accounts for the inhomogeneous temperature field in the boundary layer. We can treat this equation as an ODE, with the understanding that integration constants may actually be slowly varying functions of time.

Crystallinity profile: The differential equation for the crystallinity profile may have many possible solutions but we focus on the simplest case where $f(s) = 0$ and examine two limiting cases:

1. When $\phi_0^i \to 0$ we can approximate eqn. 20 as

$$-\frac{\partial^2}{\partial s^2}\phi_0^i + \phi_0^i \simeq 0. \tag{21}$$

The solution of this ordinary differential equation valid for crystallinity very close to the phase boundary is obtained as

$$\phi_0^i \simeq \sinh s, \tag{22}$$

where the boundary condition $\phi_0^i(0) = 0$ is imposed. In other words grows as a hyperbolic sin function. This form also indicates that $\frac{\partial \phi}{\partial s}\big|_{s=0}$ is positive. Specifying this value is equivalent to specifying the heterogeneous nucleation rate for crystallisation at $s = 0$.

2. When $\phi_0^i \to 1$ we can approximate eq. 20 as

$$\frac{\partial^2}{\partial s^2} \ln(1 - \phi_0^i) \simeq -1, \qquad (23)$$

which has the solution

$$\ln\left(1 - \phi_0^i\right) \simeq -\frac{s^2}{2} + Cs + D, \qquad (24)$$

where C and D are to be determined from the boundary conditions. Clearly, the above solution automatically satisfies $\lim_{s \to \infty} \phi_0^i = 1$ irrespective of the values of C and D. Forcing the solution to satisfy the boundary conditions on the right hand side of the boundary layer, (i) $\phi_0^i(0) = 0$ and (ii) $\frac{\partial \phi}{\partial s}\big|_{s=0} > 0$ we obtain $C = -\frac{\partial \phi}{\partial s}\big|_{s=0}$ and $D = 0$ and hence,

$$\phi_0^i \simeq 1 - e^{-\frac{s^2}{2} - \frac{\partial \phi}{\partial s}\big|_{s=0} s}. \qquad (25)$$

Since the term in the exponent can be converted to a perfect square (see below), the crystallinity profile in the boundary layer is Gaussian in s but approximates to a hyperbolic sin behaviour as the solid - melt phase boundary is approached. However it is interesting to note that, though derived for the special case of $\phi_0^i \to 1$, eqn. 25 satisfies the boundary conditions at both $s = 0$ and $s = 1$, thus posing as an approximate solution for ϕ_0^i in the entire boundary layer. Therefore we take eqn. 25 to represent the crystallinity profile in the entire boundary layer and proceed with determining the temperature profile. Later on we will show that this approach of using eqn. 25 is not a limitation to the main conclusions derived in this work (see section 3.4).

Another point to be noted is that $\phi_0^i \to 1$ is automatically satisfied at the left edge of the boundary layer, $s \to \infty$. It justifies our earlier presumption in section 3.2.1 that corrections to $\phi_0^o(x,t) = 1$ in the outer region are identically zero.

Temperature profile: To calculate the temperature profile in the boundary layer, we substitute eqn. 19 and eqn. 25 in eqn. 18,

$$\frac{\partial^2 T_0^i(s,t)}{\partial s^2} - e^{-\frac{s^2}{2} - \frac{\partial \phi}{\partial s}\big|_{s=0} s} T_0^i = 0. \qquad (26)$$

This equation explicitly expresses the dominant thermal physics in the boundary layer: latent heat generated by crystallization (second term on the left) is conducted out of the boundary layer into the outer region (first term on the left). It is immediately clear from the former term that all the latent heat is released within the boundary layer for s on the order 10^1 where the curvature in the temperature profile (associated with conduction) is non-zero. The equation makes clear the the temperature profile becomes linear in the far field of the boundary layer. To obtain a simple analytical expression for T_0^i we rewrite eqn. 26 as

$$\frac{d^2 T_0^i}{ds^2} = \Omega \sqrt{\frac{\pi}{2}} \operatorname{erfc}\left(\frac{B}{\sqrt{2}}\right) \delta\left(s - \frac{1}{\Omega}\right) T_0^i, \qquad (27)$$

where $\Omega = e^{\frac{1}{2}B^2}$, $B = \frac{\partial \phi}{\partial s}\big|_{s=0}$ and δ is the Dirac delta function (see appendix A.3.1 for details). This transformation involves re-

placing the Gaussian-like thermal forcing function spread over s of order unity, that represents the latent heat released during crystallisation, with an *equivalent* Dirac delta function applied at a mean location $\frac{1}{\Omega}$. The Dirac delta function has the same strength as the original distribution which is ensured from the equality, $\Omega \int_B^\infty e^{-\frac{p^2}{2}} dp = \Omega \sqrt{\frac{\pi}{2}} \operatorname{erfc} \frac{B}{\sqrt{2}}$.

Hence, for $0 < s < \frac{1}{\Omega}$ and $\frac{1}{\Omega} < s < \infty$ the temperature has two separate but individually linear variations in the boundary layer. The resulting piecewise continuous temperature profile is

$$T_0^i(s,t) = E\left[s + \sqrt{\frac{\pi}{2}} \operatorname{erfc}\left(\frac{B}{\sqrt{2}}\right)\left(s - \frac{1}{\Omega}\right) \mathscr{H}\left(s - \frac{1}{\Omega}\right)\right], \qquad (28)$$

where $E = \frac{\partial T}{\partial s}\big|_{s=0}$ and $\mathscr{H}$ is the Heaviside step function. The boundary conditions $T_0^i(0,t) = 0$ and $\frac{\partial T}{\partial s}\big|_{s=0} > 0$ have been applied in obtaining this expression. This transformation make solution of the boundary layer temperature profile very straightforward. It should be emphasized that the important thermal features (far-field temperature profile in the boundary layer, the behavior of the temperature at the location of the pulse) are *insensitive* to the details of the equivalent pulse, provided the magnitude of latent heat released is correct, and the pulse is located at a value of s of order unity. The the behavior of the temperature at the location of the pulse leads to a confirmation of the Gryte-Lovinger ansatz. It is interesting to note that the linear variation near the left edge of the boundary layer can be anticipated from eqn. 26. In other words, in the limit of $(s \to \infty)$ eqn. 26 has the form $\frac{\partial^2 T(s,t)}{\partial s^2} \simeq 0$ which predicts a linear variation of temperature T with the boundary layer coordinate s. This functional form of temperature ensures the smooth matching of the temperature profile in the outer and the boundary layer.

3.2.3 Matching the outer and the inner layer solutions

In earlier sections, we obtained the analytical expressions describing the temperature and the crystallinity profiles in the outer and the boundary layer separately. During this procedure, α in eqn. 16 and E in eqn. 28 remain as undetermined constants. Moreover, the location of the solid–melt boundary $\delta(t)$ is not calculated yet. To evaluate these undetermined quantities we follow Van Dyke procedure where the temperature profiles in the boundary layer and the outer layer are matched[9]. As noted earlier the crystallinity profiles inside the boundary layer and the outer layer are already in agreement with each other.

Towards the matching procedure, we rewrite the outer solution eqn. 16. in terms of the inner variable $z = \delta(t) - \sqrt{\varepsilon}s$. Exploiting the smallness of the variable ε, eqn. 16 is expanded as a Taylor series to obtain the temperature profile in the outer region as (see appendix A.3.2 for details)

$$T_0^o(x,t) \simeq 1 - \alpha \left[\operatorname{erf}\left(\frac{\delta(t)}{2\sqrt{t}}\right) - \frac{1}{\sqrt{\pi}} e^{-\left(\frac{\delta(t)}{2\sqrt{t}}\right)^2} \frac{\sqrt{\varepsilon}}{\sqrt{t}} s\right]. \qquad (29)$$

Similarly, in the boundary layer we take the limit of $s \to \infty$ to perform the matching procedure. Therefore, in this limit, and when $B << 1$ we rewrite the boundary layer temperature profile

(eqn. 28) as

$$T(s,t) \simeq E\left\{\left[1 + \sqrt{\frac{\pi}{2}}\right]s - \sqrt{\frac{\pi}{2}}\right\}. \tag{30}$$

Matching the two solutions, and thus equating the coefficients of terms of similar powers of s we obtain,

$$\delta(t) = 2\beta\sqrt{t}, \tag{31}$$

$$\alpha = \frac{1 + E\sqrt{\frac{\pi}{2}}}{\operatorname{erf}\beta}, \tag{32}$$

where β is a constant yet to be determined.

The solid–melt phase boundary: With the above matching the temperature profile in the outer region, in the asymptotic limit of ε, may be written as

$$T_0^o \simeq \frac{1 + E\sqrt{\frac{\pi}{2}}}{\sqrt{\pi}} \frac{e^{-\beta^2}}{\operatorname{erf}\beta} \frac{\sqrt{\varepsilon}}{\sqrt{t}} s - E\sqrt{\frac{\pi}{2}}.$$

This temperature profile in the outer region will match with the inner solution only if the coefficient multiplying s is $O(\varepsilon^0)$. Hence we may write $\beta = \gamma\sqrt{\varepsilon}$ where γ is an $O(10^0)$ numerical constant. Thus we determine the location of the solid–melt boundary as

$$\delta(t) = 2\gamma\sqrt{\varepsilon t}. \tag{33}$$

$\gamma = \frac{1}{\sqrt{2}}$ can be taken to facilitate comparison with the Stefan model (see section 3.3).

Complete set of solutions: Simplifying the matching conditions, eqns. 31-32 we find that

$$E = \frac{1}{\sqrt{2t}\left(1 + \sqrt{\frac{\pi}{2}}\right) - \sqrt{\frac{\pi}{2}}}. \tag{34}$$

This is a remarkably simple result since $E = \frac{\partial T}{\partial s}\big|_{s=0}$ which indicates that the temperature gradient at the solid-melt region ($s = 0$) decays algebraically with time.

Then complete set of solutions in the outer and inner layer are

$$T_0^o(z,t) = 1 - \frac{z}{\delta(t)} - \frac{\sqrt{\frac{\pi}{2}}}{\sqrt{2t}\left(1 + \sqrt{\frac{\pi}{2}}\right) - \sqrt{\frac{\pi}{2}}} \frac{z}{\delta(t)}, \tag{35}$$

$$\phi_0^o(z,t) = 1, \tag{36}$$

$$T_0^i(s,t) \simeq \frac{1}{\sqrt{2t}\left(1 + \sqrt{\frac{\pi}{2}}\right) - \sqrt{\frac{\pi}{2}}}\left[s + \sqrt{\frac{\pi}{2}}\ (s-1)\ H\ (s-1)\right], \tag{37}$$

$$\phi_0^i(s,t) \simeq 1 - e^{-\frac{s^2}{2} - \frac{\partial \phi}{\partial s}\big|_{s=0} s}. \tag{38}$$

Note that only a pseudo-steady form for temperature in the outer layer, $T_0^o(z,t)$, of eqn. 16, arises naturally in the solution since transient terms involving $\delta'(t) = \sqrt{\frac{\varepsilon}{2t}}$ are neglected in formulating boundary layer equations. In other words, the presumption of $\delta'(t) << \sqrt{\varepsilon}$ or equivalently, $\sqrt{2t} >> 1$ is built into the calcu-

lations. This is a requirement for a psuedo steady solution for $T_0^o(z,t)$ appearing above. Similarly, although T shows a non-trivial variation in both the outer and inner regions, the evolution of ϕ occurs completely within the boundary layer. This evolution is assumed to be completely described by the last equation, for $\phi_0^i(s,t)$.

3.2.4 Composite Solution

Considering that the solutions in each region are completely derived, a composite solution can be constructed as follows. The temperature profile T follows from

$$T^{comp} = T_0^o + T_0^i - \lim_{s\to\infty} T_0^i. \tag{39}$$

Replacing s in terms x using its definition and simplifying for the inner and outer temperature profiles we obtain the composite solution for temperature as

$$T^{comp} = 1 - \bar{z} - \frac{\sqrt{\frac{\pi}{2}}}{\sqrt{2t}\left(1 + \sqrt{\frac{\pi}{2}}\right) - \sqrt{\frac{\pi}{2}}}\left(\bar{z} - \left(\sqrt{2t}\,(1-\bar{z}) - 1\right)\right.$$
$$\left.\left[H\left(\sqrt{2t}\,(1-\bar{z}) - 1\right) - 1\right]\right), \tag{40}$$

where $\bar{z} = \frac{z}{\delta(t)}$. Similarly, the composite solution for ϕ may be written by combining eqns. 36 and 38 as

$$\phi^{comp} = 1 - e^{-t(1-\bar{z}) - B\sqrt{2t}(1-\bar{z})}. \tag{41}$$

This composite solution is strictly valid only under the psuedo steady state limit, i.e, when $\frac{1}{\sqrt{2t}} << 1$. Similarly, for matching purposes we have assumed that the crystallinity profile near the phase boundary, $\frac{\partial \phi}{\partial s}\big|_{s=0}$ is small. These approximations have been advantageous as they helped to perform the analytical operations and to obtain the above discussed solution. We demonstrate the validity of our solution (i) by reducing it to the Stefan model in the appropriate limit and (ii) then validating the Lovinger–Gryte hypothesis, as described in the next two sections.

3.3 Comparison with Stefan's Model

As described in section 2.1, the Stefan model of a moving phase boundary for simple molecules in one dimension is a classical result in heat transfer. In this case, there exists a sharp boundary between the solid and the melt phases and the crystallinity profile reduces to a step function. The heat released during the crystallisation is transferred to the solid layer via conduction giving rise to the well known boundary condition,

$$k\left.\frac{\partial}{\partial z}T\right|_{z=\Delta(t)} = \rho\hat{L}\phi_m\frac{d}{dt}\Delta. \tag{42}$$

The above expression contains dimensional variables. $\hat{L}$ is the latent heat of crystallisation, ϕ_m is the extent of crystallinity in the solid phase which is a constant and Δ is the location of the solid–melt phase boundary.

Stefan's solution[8] is given by

$$\bar{T} = \frac{T_m - T}{T_m - T_o} = 1 - \frac{\operatorname{erf}\eta}{\operatorname{erf}\gamma}, \tag{43}$$

where $\eta = \frac{x}{2\sqrt{\hat{\alpha}t}}$ is the similarity variable, $\hat{\alpha}$ is the thermal diffusivity and $\lambda = \frac{\hat{L}\phi_m}{\hat{C}(T_m - T_o)}$ is the non-dimensional parameter arising in the formulation. In the above, the constant γ needs to be determined as a solution to the transcendental equation $\lambda = \frac{e^{-\gamma^2}}{\sqrt{\pi}\gamma\operatorname{erf}\gamma}$. The location of the phase boundary can be determined as $\Delta(t) = 2\gamma\sqrt{\hat{\alpha}t}$.

We now note that the pseudo steady state limit exists when $t >> \frac{\Delta^2}{\alpha}$, i.e, when $\lambda >> 1$ (see appendix A.4 for details). Under these conditions the equation defining γ simplifies to give $\gamma << 1$ so that $e^{\gamma^2} \simeq 1$ and $\operatorname{erf}\gamma \simeq \frac{2}{\sqrt{\pi}}\gamma$ leading to $\gamma \simeq \sqrt{\frac{\varepsilon}{2}}$. Analogously, the similarity variable evaluated at the phase boundary can be approximated as $\frac{z}{2\sqrt{\alpha t}} \simeq \sqrt{\frac{\varepsilon}{2}}$. Therefore, we obtain the simplified form of Stefan's similarity solution from eqn. 43 as

$$\bar{T} = 1 - \frac{z}{\Delta(t)}. \tag{44}$$

Scaling the numerator and the denominator of the second term by the length scale d, we obtain $\bar{T} = 1 - \frac{\bar{z}}{\delta(t)}$ which indicates that the pseudo steady solution for temperature in the Stefan model is identical to the leading order approximation in the boundary layer crystallisation model discussed in the previous sections (eqns. 35 and 37 in the limit of $t >> 1$ and $\lambda >> 1$ both reduce to eqn. 44). It only remains to show that the Stefan model solution for $\Delta(t)$ when $\lambda >> 1$ (psuedo steady limit) matches that at leading order from the crystallisation boundary layer model in the same limit. This is easily achieved by noting that when $\lambda >> 1$, the Stefan model gives, $\Delta(t) \simeq \sqrt{2\varepsilon\alpha t}$ and therefore, $\frac{\Delta}{d} = \delta \simeq \sqrt{2\varepsilon\bar{t}}$ which exactly matches the result from the boundary layer crystallisation model (eqn. 33 with $\gamma = \frac{1}{\sqrt{(2)}}$).

3.4 Lovinger–Gryte hypothesis

In the boundary layer crystallisation model, the solution for the temperature profile is obtained as a piece-wise continuous function, determined by localizing the thermal "forcing" term as an equivalent Dirac pulse. The temperature at the location of the pulse, $s = 1$, where all the crystallisation effectively takes place can be determined as

$$T_0^i(s = 1, t) \simeq \frac{\delta'(t)}{\sqrt{\varepsilon}} \frac{1}{1 + \sqrt{\frac{\pi}{2}}}. \tag{45}$$

In eqn. 45, we have replaced $\frac{1}{\sqrt{2t}}$ by $\frac{\delta'(t)}{\sqrt{\varepsilon}}$. As in previous sections the usual approximations, namely, (i) the pseudo steady state limit, $\sqrt{2t} >> 1$ and (ii) $B = \frac{\partial\phi}{\partial s}\big|_{s=0}$ is sufficiently small are utilised in deriving eqn. 45 as well.

Note that larger values of $T_0^i(s = 1)$ indicate larger undercooling (note that T is a scaled quantity). Therefore, eqn. 45 shows that the effective undercooling for crystallisation scales with the front speed $\delta'(t)$. This is an important conclusion arising form our calculations because this result is consistent with the Lovinger–Gryte
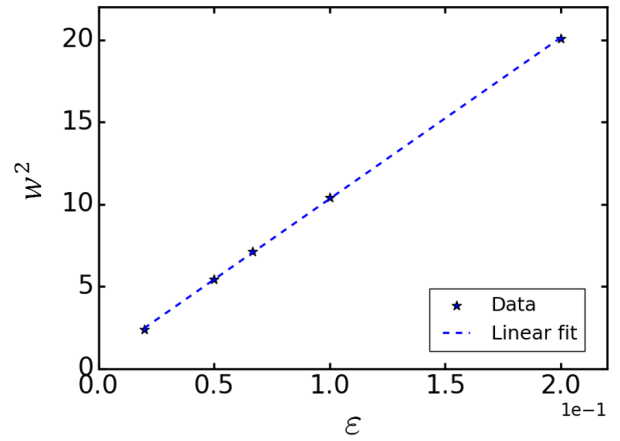
Fig. 2 Variation in the boundary layer thickness, w, plotted as a squared quantity, with the small parameter ε used in the boundary layer analysis. Symbols are data obtained from numerical simulations and the dashed line is a linear fit. The boundary layer thickness is determined in the simulations as the region where $0.001 < \phi < 0.999$.

hypothesis that the front speed sets the effective undercooling.

We now demonstrate that the same conclusion arises even if we do not assume the localised thermal forcing model. Near the phase boundary in the limit of $\phi << 1$ and $s << 1$, we can obtain the crystallinity from eqn. 25 and the temperature from eqn. 69 in the appendix as

$$\phi \simeq B s \tag{46}$$

$$T \simeq \frac{\delta'(t)}{\sqrt{\varepsilon}\left(1 + \sqrt{\frac{\pi}{2}}\right)}\left[\sinh\left(\frac{\phi}{B}\right) - B\cosh\left(\frac{\phi}{B}\right)\right]. \tag{47}$$

The last expression demonstrates that very near the moving front, a fixed value of ϕ corresponds to a fixed value of $\frac{T}{\delta'(t)}$. In other words,

$$T \sim \delta'(t) \text{ for fixed } \phi << 1 \text{ ; } s << 1 \text{ ; } \sqrt{2t} >> 1, \tag{48}$$

again indicating that effective undercooling for crystallisation scales with the front speed, namely Lovinger–Gryte hypothesis.

4 Comparison with numerical solution

In this section, we compare the analytical results obtained in the previous sections with full numerical solutions. To numerically solve eqns. 4-5, the technique of method of lines was adopted. More details are reported in[7]. The system considered is same as that illustrated in Fig. 1. Thus, based on the non-dimensionalisation introduced in section 2.2, the temperature varies from $T = 1$ at $z = 0$ to $T = 0$ at $z = \delta(t)$. Correspondingly the crystallinity varies from $\phi = 1$ at $z = 0$ to $\phi = 0$ at $z = \delta(t)$. Both temperature and crystallinity are zero in the melt region, i.e., for $z > \delta(t)$.

A crucial assumption that led to the successful development of the boundary layer analysis for the problem under consideration is the choice of $c = \frac{1}{2}$ in eqn. 17. This choice led to the proper

(a)

(b)
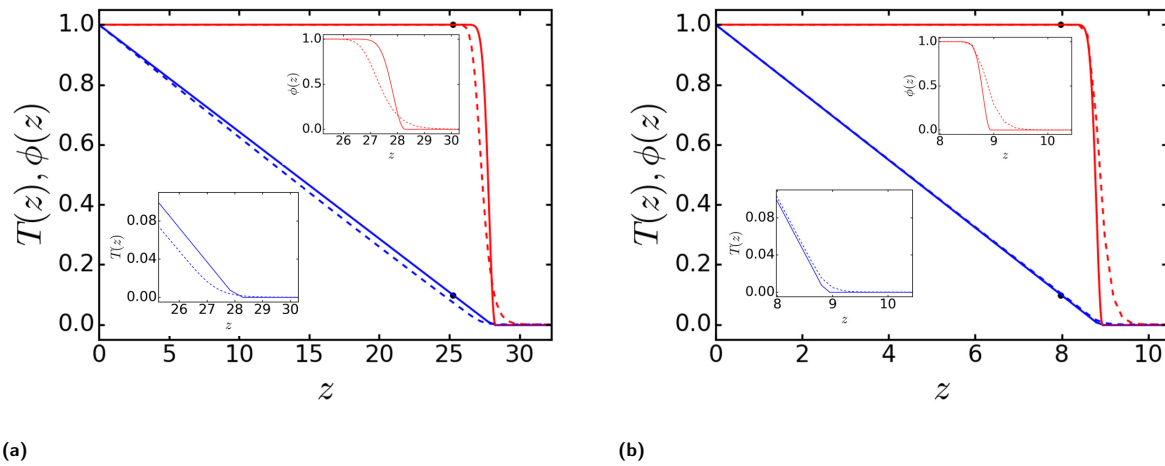
Fig. 3 Comparison of analytical results (solid lines) with numerical solutions (dashed lines) for (a) $\varepsilon = 0.2$, and (b) $\varepsilon = 0.02$. The blue lines show the temperature, T, profiles whereas the red lines are the corresponding crystallinity, ϕ, profiles. The boundary between the outer and the inner region (where crystallinity starts to fall down from 1) are marked by thick black dots on the temperature and crystallinity profiles. The insets show the magnified view of temperature and the crystallinity profiles across the boundary layer. In the analytical calculations we use $B = 0.001$, $\gamma = 1/\sqrt{2}$, and $t = 2000$.

rescaling of the boundary layer coordinates resulting a dominant balance between conductive flux and the heat released during crystallisation. Therefore, we firstly verify and show that this choice is indeed correct and the boundary layer thickness varies as square root of the small variable ε used in the analysis. Fig. 2 shows the results from numerical simulations where the width of the boundary layer is plotted as a function of ε. The boundary layer thickness w is estimated as that length of the solidified region in which $0.001 < \phi < 0.999$. The square of w plotted as a function of ε in Fig. 2 is a straight line indicating that $w \sim \sqrt{\varepsilon}$, thus validating the rescaling of the boundary layer coordinate adopted in the analytical developments reported in the previous sections.

Next, we compare the temperature and crystallinity profiles calculated from the analytical solution with the profiles obtained from full numerical simulations. Fig. 3 shows this comparison for two different values of ε. In these plots, solid lines correspond to analytical solutions and the dashed lines correspond to numerical solutions. The profiles in the entire domain (both inner and outer regions) are shown in the plots, and the thick black dots in the temperature and the crystallinity profiles demarcate the inner and the outer region. The profiles in the boundary layer region are magnified and shown in the two insets. The plots correspond to the long time limit, *i.e, t >> 1*. We have also verified that the analytical solutions given in this figure are independent of the choice of B as long as $B << 1$. As expected, in both figures, the non-dimensional temperature and the crystallinity vary from unity at $z = 0$ to zero for $z \geq \delta(t)$.

The analytical solutions, especially for the crystallinity profile, are not accurate in the boundary layer. Note that the exact solution of the driving differential equations are, of course, the ones that yield the "exact" numerical solutions; hence the errors are a consequence of the approximations made to facilitate the analytical solution. However, the temperature at the point where the Dirac pulse is introduced, i.e., the effective temperature in a hypothetical system with a square well crystallinity profile, tracks

the exact answers (Fig. 4). Again, the agreement is qualitative, but the important point is that the analytical solution provides a means to understand the Lovinger-Gryte ansatz that the crystallisation occurs at an effective velocity dependent isothermal protocol. Thus, our analytical solutions capture the essential physics of these situations.
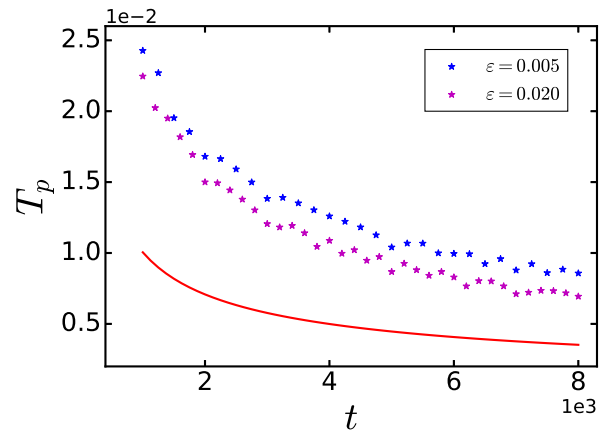
Fig. 4 Temperature at the pulse position, T_p, versus time, t, from theory (red solid line) and simulations (symbols) for two different values of ε (listed in the legend). Note that T_p from theory is independent of ε.

Finally, we consider the Lovinger–Gryte hypothesis, the relationship between the velocity of the moving front and the corresponding temperature, by comparing the analytical and numerical solutions. As explained in section 3.4, eqn. 48 predicts that the temperature of the moving front increases with increase in the growth velocity. The data obtained from the simulations are shown in Fig. 5 which is in agreement with eqn. 48. Moreover, the data shown in Fig. 5 corresponds to simulations performed at various values of ε. However, it can be seen that, on renormalising the temperature of the moving front, the data col-
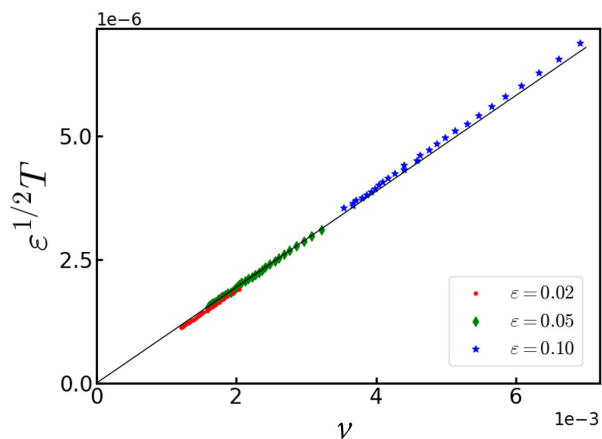
Fig. 5 Dependence of temperature of the moving front (the solid-melt phase boundary) on the growth velocity v. The symbols are data from simulations for various values of ε, and hence temperature is scaled with $1/\sqrt{\varepsilon}$. The black solid line passing through the origin is drawn for a visual guidance to illustrate the linear dependency of temperature on velocity of the moving front. The moving front is determined as the location at which $\phi = 0.001$ and the temperature and velocity at this point are used in this plot. The data also corresponds to the long time limit ($t > 1000$).

lapses to a single curve, suggesting that the scaling relation is $T\sqrt{\varepsilon} \sim \delta'(t)$, again consistent with the predictions made in section 3.4. Thus, the analytical predictions are in agreement with the numerical solutions. It must be remembered that T refers to the non-dimensional temperature $\frac{T_m - T}{T_m - T_l}$. Hence an increase in T in Fig. 5 corresponds to a decrease in the actual temperature, *i.e*, the temperature of the crystallising front of a polymer melt decreases with the growth velocity, which is the Lovinger–Gryte hypothesis.

5 Conclusion

We develop a theoretical framework, and an associated approximate boundary layer solution, for the Stefan problem modified to model polymer crystallisation, which is not instantaneous, but rather whose kinetics follow an Avrami-like form. The analytical results are consistent with previous numerical work and with the ansatz of Lovinger and Gryte who proposed that each zone annealing speed corresponds to an effective isothermal crystallisation temperature. This result arises because the enthalpy of crystallization, which is distributed over the whole zone undergoing crystallization, appears to be concentrated into a point source in the context of the equations determining the temperature profile. In addition, the analytical calculation also predicts the previously observed behavior of identical evolution of crystal growth-front in the Stefan problem and an equivalent polymer crystallisation problem in the limit of large latent heat capacity. This work also illustrates the boundary layer approximation as a powerful tool to solve coupled differential equations in asymptotic limits.

This work considers only the case of a stationary sink: the case with a moving sink, which more closely models zone annealing experiments, is not included and will be addressed in the following paper.

6 Conflicts of interest

The authors declare no competing financial interests.

7 Acknowledgments

References

1 W. Pfann, *Science*, 1962, **135**, 1101–1109.
2 W. Tiller, K. Jackson, J. Rutter and B. Chalmers, *Acta Metallurgica*, 1953, **1**, 428–437.
3 A. J. Lovinger and C. C. Gryte, *Macromolecules*, 1976, **9**, 247–253.
4 A. J. Lovinger, C.-M. Lau and C. C. Gryte, *Polymer*, 1976, **17**, 581–586.
5 A. J. Lovinger and C. C. Gryte, *Journal of Applied Physics*, 1976, **47**, 1999–2004.
6 A. A. Krauskopf, A. M. Jimenez, E. A. Lewis, B. D. Vogt, A. J. Müller and S. K. Kumar, *ACS Macro Letters*, 2020, **9**, 1007–1012.
7 S. Adhikari, A. Purushothaman, A. A. Krauskopf, C. Durning, S. K. Kumar and S. P. Thampi, *Soft Matter*, 2021, **17**, 2518–2529.
8 J. Stefan, *Annalen der Physik*, 1891, **278**, 269–286.
9 W. M. Deen, *Analysis of transport phenomena*, Oxford university press New York, 1998.
10 M. Avrami, *The Journal of chemical physics*, 1939, **7**, 1103–1112.
11 M. Avrami, *The Journal of chemical physics*, 1940, **8**, 212–224.

A Appendix

A.1 Derivation of Avrami crystallization kinetics

In this section, we recap the Avrami formulation[10,11] for crystallization kinetics to clarify our adaptation of it for the case of crystallization in a thermal field. We derive the Avrami formula for growing particles of dimension, d, and obtain a general equation for the rate of crystallization. The equation used in this study corresponds to $d = 1$, and all the nuclei are born at once (heterogeneous nucleation).

Following a sudden *uniform* quench to a fixed undercooling, crystallization happens via nucleation and crystal growth, which in general occur simultaneously. If only a minor change in density occurs upon solidification, we can assume the total volume of the system $V_{tot}[=]L^d$ is constant. with d indicating the space dimensionality of the system. Let dN denotes the number of nuclei spawned during a time interval dt' at time t'. If the solid particles grow linearly with time, then the size (characterized by a length) of those nuclei at time t is $g(t - t')$ where g is a constant. Then, instantaneous rate of change of space occupied by solid material, V_c, at a time t in a d dimensional space is

$$dN(t')m(d)\frac{d}{dt}\left(g(t-t')\right)^d = dN(t')m(d)g^d d(t-t')^{d-1}, \quad (49)$$

where $m(d)$ is a dimensionless geometric constant depending on the dimesionality (e.g. $m(1) = 1$, $m(2) = 4\pi$, $m(3) = 4\pi/3$ for centro-symmetric particles). The total rate of change of V_c at time t is the result of the current rate of growth of all particles born from $t = 0$

$$\frac{dV_c}{dt} = d\, m(d) \int_0^t dt' \frac{dN(t')}{dt'} g^d (t-t')^{d-1}. \qquad (50)$$

The above eqn. does not account for particle impingement. A simple (mean-field) correction is to multiply the rhs by the current fraction of space unoccupied by solid:

$$\frac{1}{1-\phi}\frac{dV_c}{dt} = d\, m(d) \int_0^t dt' \frac{dN(t')}{dt'} g^d (t-t')^{d-1}. \qquad (51)$$

This relation leads to several well known forms of Avrami's law when taking appropriate assumptions for the nucleation process. For example, heterogeneous nucleation might be modeled as

$$\frac{dN(t')}{dt'} = N_0 \delta(t'), \qquad (52)$$

where N_0 is a constant. It leads to

$$\frac{1}{1-\phi}\frac{dV_c}{dt} = N_0\, d\, m(d)\, g^d t^{d-1}. \qquad (53)$$

For $d = 3$ one recovers a common form of Avrami's law

$$\phi = 1 - e^{-\frac{4\pi}{3} g^3 \frac{N_0}{V_{tot}} t^3}, \qquad (54)$$

where V_c was eliminated by using $\phi = \frac{V_c}{V_{tot}}$. Importantly, regardless of d, one recovers a *differential equation* for the case of instantaneous, heterogeneous nucleation, *even if the temperature is allowed to vary* (note g is temperature dependent). This points to simple, tractible modeling via partial differential equations for the case of solidification in a *thermal field*. We adopt the presumption of instantaneous heterogeneous nucleation in what follows. By contrast for homogeneous nucleation one only recovers a differential equation if g is treated as constant, otherwise an integro-differential equation results, where a memory integral keeping track of $g(t')$ through the temperature history is needed.

The crystallization kinetic equation is even simpler for $d = 1$,

$$\frac{1}{1-\phi}\frac{d\phi}{dt} = g\frac{N_0}{V_{tot}}, \qquad (55)$$

which is a reasonable presumption for systems where the crystallizing particles grow along one spacial direction, which is the case for crystallization in a zone refining process[4,6]. Note, if one takes the limit $t \to 0_+$, for the last equation, inherent is the condition

$$\left.\frac{d\phi}{dt}\right|_{t=0} = g\frac{N_0}{V_{tot}} > 0 \qquad (56)$$

which justifies the boundary condition we take on the fraction crystallized (see equation (22) and the ensuing discussion in the text).

Clearly, for heterogeneous nucleation and 1-d solid particle growth, the above equation applies locally, justifying a direct adaptation to the case of an inhomogeneous, time dependent thermal field. In particular, for the case of a thermal field we make the replacements

$$\frac{d\phi}{dt} \to \frac{\partial\phi}{\partial t}, \qquad (57)$$

$$g\frac{N_0}{V_{tot}} = F(T) \to R\frac{T_m - T}{T_m} \qquad (58)$$

where eqn. 58 implies weak undercooling.

A.2 Transformation of the governing equations to the boundary layer coordinate s

To write the differential eqns. 4-5 in term of the boundary layer coordinate s,

$$df(x,t) = \left(\frac{\partial f}{\partial t}\right)_x dt + \left(\frac{\partial f}{\partial x}\right)_t dx = \left(\frac{\partial g}{\partial t}\right)_s dt + \left(\frac{\partial g}{\partial s}\right)_t ds = dg(s,t),$$

$$\left.\frac{df}{dt}\right|_x = \left(\frac{\partial f}{\partial t}\right)_x = \left(\frac{\partial g}{\partial t}\right)_s + \left(\frac{\partial g}{\partial s}\right)_t \left.\frac{ds}{dt}\right|_x. \qquad (59)$$

Then, it follows

$$\left(\frac{\partial T(x,t)}{\partial t}\right)_x = \left(\frac{\partial T(s,t)}{\partial t}\right)_s + \frac{1}{\varepsilon^c}\left(\frac{\partial T(s,t)}{\partial s}\right)_t \delta'(t), \qquad (60)$$

$$\frac{\partial}{\partial t}\phi(x,t) = \left(\frac{\partial\phi(s,t)}{\partial t}\right)_s + \frac{1}{\varepsilon^c}\left(\frac{\partial\phi(s,t)}{\partial s}\right)_t \delta'(t). \qquad (61)$$

Also

$$\left.\frac{df}{dx}\right|_t = \left(\frac{\partial f}{\partial x}\right)_t = \left(\frac{\partial g}{\partial s}\right)_t \left.\frac{ds}{dx}\right|_t,$$

so that

$$\left(\frac{\partial T(x,t)}{\partial x}\right)_t = -\frac{1}{\varepsilon^c}\left(\frac{\partial T(s,t)}{\partial s}\right)_t, \qquad (62)$$

and

$$\left(\frac{\partial^2 T(x,t)}{\partial x^2}\right)_t = \frac{1}{\varepsilon^{2c}}\left(\frac{\partial^2 T(s,t)}{\partial s^2}\right)_t. \qquad (63)$$

Using eqns. 60-63 in eqns. 4-5, the governing equations in the boundary layer become

$$\varepsilon^{1+c}\frac{\partial T(s,t)}{\partial t} + \varepsilon\delta'(t)\frac{\partial T(s,t)}{\partial s} = \varepsilon^{1-c}\frac{\partial^2 T(s,t)}{\partial s^2} - \varepsilon^c\frac{\partial\phi(s,t)}{\partial t} - \delta'(t)\frac{\partial\phi(s,t)}{\partial s}, \qquad (64)$$

and

$$\varepsilon^c\frac{\partial\phi(s,t)}{\partial t} + \delta'(t)\frac{\partial\phi(s,t)}{\partial s} = \varepsilon^c(1-\phi)T. \qquad (65)$$

A.3 Temperature profile in the boundary layer

A.3.1 Introduction of a Dirac pulse in the governing differential equation

The heat equation in the boundary layer in the first approximation (eqn. 26 in the main text) is

$$\frac{\partial^2 T(s,t)}{\partial s^2} - e^{-\frac{s^2}{2} - \left.\frac{\partial\phi}{\partial s}\right|_{s=0} s} T = 0, \qquad (66)$$

where we have again dropped super and subscripts.

We treat the boundary layer equation for T like an ode with the understanding that integration constants may be (slowly

varying) functions of time. First note that the combination $-\frac{s^2}{2} - \frac{\partial \phi}{\partial s}\big|_{s=0}\, s = -\frac{s^2}{2} - Bs$ appears in the differential equation for T, which can be rewritten as $-(\frac{s}{\sqrt 2} + \frac{\sqrt 2}{2}B)^2 + \frac{1}{2}B^2$ so that

$$e^{-\frac{s^2}{2} - \frac{\partial \phi}{\partial s}\big|_{s=0} s} = \exp{-(\frac{s}{\sqrt 2} + \frac{\sqrt 2}{2}B)^2}\exp{\frac{1}{2}B^2} \ ; \ B = \frac{\partial \phi}{\partial s}\Big|_{s=0}.$$

Putting

$$p = s + B$$

leads to

$$\frac{\partial^2 T}{\partial p^2} - \Omega\, e^{-\frac{p^2}{2}} T = 0; \tag{67}$$

$$\Omega = e^{\frac{1}{2}B^2}, B = \frac{\partial \phi}{\partial s}\big|_{s=0}$$

subject to

$$T(p = B, t) = 0 \ , \ B = \frac{\partial \phi}{\partial s}\Big|_{s=0},$$

and an additional boundary condition. The behavior for small $s = \varepsilon << 1 (\Rightarrow p = B + \varepsilon \ ; \ \varepsilon << 1)$ resembles that for $\phi = \varepsilon << 1$ discussed above in that the governing equation for T is the same as that for ϕ, $\frac{\partial^2 T}{\partial p^2} \simeq T$, giving

$$T \simeq C \sinh(B+s) + D \cosh(B+s), \tag{68}$$

where $B = \frac{\partial \phi}{\partial s}\big|_{s=0}$, C and D are integration "constants" (actually they depend on t). Applying $T(s=0,t) = 0 \Rightarrow T(p=B,t)=0$ eventually gives

$$T \simeq E\,[\cosh B \sinh(B+s) - \sinh B \cosh(B+s)], \tag{69}$$

where $B = \frac{\partial \phi}{\partial s}\big|_{s=0}$, and $E = \frac{\partial T}{\partial s}\big|_{s=0}$. Notice that if one insists $T(0,t) = 0$ then $\frac{\partial T}{\partial s}\big|_{s=0} > 0$ in order to have a nontrivial solution. These considerations encourage the second auxiliary condition be $\frac{\partial T}{\partial s}\big|_{s=0} > 0$.

This equation governing T in the boundary layer is difficult to solve, even asymptotically. A simple approach is to replace the "pulse" $\Omega\, e^{-\frac{p^2}{2}}$ by an equivalent Dirac applied at the mean value of p under the pulse. The equivalent Dirac magnitude is

$$\Omega \int_B^\infty e^{-\frac{p^2}{2}}\, dp = \Omega\sqrt{\frac{\pi}{2}}\, \mathrm{erfc}\,\frac{B}{\sqrt 2} \ ; \ B = \frac{\partial \phi}{\partial s}\Big|_{s=0},$$

and the Dirac should be applied at

$$p_0 = B + \int_B^\infty p\, e^{-\frac{p^2}{2}}\, dp = B + e^{-\frac{1}{2}B^2} = B + \frac{1}{\Omega} \ ; \ \Omega = e^{\frac{1}{2}B^2} \ ; \ B = \frac{\partial \phi}{\partial s}\Big|_{s=0}.$$

So an equivalent Dirac pulse is

$$\Omega\, e^{-\frac{p^2}{2}} \ \rightarrow \ \Omega\sqrt{\frac{\pi}{2}}\, \mathrm{erfc}\,\frac{B}{\sqrt 2}\ \delta(p-p_0);$$

$$\Omega = e^{\frac{1}{2}B^2}, B = \frac{\partial \phi}{\partial s}\Big|_{s=0}, \ \text{and}\ p_0 = B + \frac{1}{\Omega}.$$

Consequently we replace the original system (eqn. 67) by

$$\frac{d^2 T}{dp^2} = \Omega\sqrt{\frac{\pi}{2}}\, \mathrm{erfc}\left(\frac{B}{\sqrt 2}\right)\delta(p-p_0)\, T, \tag{70}$$

from which eqn. 27 in the main text readily follows.

A.3.2 Temperature and crystallinity profiles

For $B < p < B + \frac{1}{\Omega}$ and $B + \frac{1}{\Omega} < p < \infty$, T increases linearly and the resulting profile is piecewise continuous. So, from eqn. 70,

$$T(s,t) = E\left[s + \sqrt{\frac{\pi}{2}}\, \mathrm{erfc}\,\frac{B}{\sqrt 2}\ \left(s - \frac{1}{\Omega}\right)H\left(s - \frac{1}{\Omega}\right)\right], \tag{71}$$

where $\Omega = e^{\frac{1}{2}B^2}$; $B = \frac{\partial \phi}{\partial s}\big|_{s=0}$; $E = \frac{\partial T}{\partial s}\big|_{s=0}$.

For the purpose of matching we need

$$\lim_{s\to\infty} T(s,t) \sim E\left[1 + \sqrt{\frac{\pi}{2}}\, \mathrm{erfc}\,\frac{B}{\sqrt 2}\right]s - \frac{1}{\Omega}E\sqrt{\frac{\pi}{2}}\, \mathrm{erfc}\,\frac{B}{\sqrt 2}$$

$$\sim \frac{\partial T}{\partial s}\Big|_{s=0}\left\{\left[1 + \sqrt{\frac{\pi}{2}}\, \mathrm{erfc}\,\frac{1}{\sqrt 2}\frac{\partial \phi}{\partial s}\Big|_{s=0}\right]s \right. \tag{72}$$

$$\left. - \frac{1}{\Omega}\sqrt{\frac{\pi}{2}}\, \mathrm{erfc}\,\frac{1}{\sqrt 2}\frac{\partial \phi}{\partial s}\Big|_{s=0}\right\}.$$

Evidently taking $B \to 0$ is benign to the temperature's behavior in the boundary layer in which case

$$\lim_{s\to\infty} T(s,t) \sim \frac{\partial T}{\partial s}\Big|_{s=0}\left\{\left[1 + \sqrt{\frac{\pi}{2}}\right]s - \sqrt{\frac{\pi}{2}}\right\} \ ; \ B = \frac{\partial \phi}{\partial s}\Big|_{s=0} << 1. \tag{73}$$

Hereafter we adopted the approximation

$$\mathrm{erfc}\,\frac{1}{\sqrt 2}B \ = \ \mathrm{erfc}\,\frac{1}{\sqrt 2}\frac{\partial \phi}{\partial s}\Big|_{s=0} \simeq 1$$

for clarity in what follows, with the understanding that they can easily be relaxed, and proceed to match with the outer solution $T_0^o(x,t) = 1 - \alpha\,\mathrm{erf}\left(\frac{x}{2\sqrt t}\right)$. Using Van Dyke matching[9] we rewrite the outer solution in terms of the inner variable $s = \frac{\delta(t) - x}{\sqrt \varepsilon} \Rightarrow x = \delta(t) - \sqrt \varepsilon\, s$. Then,

$$T_0^o(x,t) = 1 - \alpha\,\mathrm{erf}\left(\frac{x}{2\sqrt t}\right) = 1 - \alpha\,\mathrm{erf}\left(\frac{\delta(t)}{2\sqrt t} - \frac{\sqrt \varepsilon s}{2\sqrt t}\right)$$

$$\simeq 1 - \alpha\left[\mathrm{erf}\left(\frac{\delta(t)}{2\sqrt t}\right) - \frac{1}{\sqrt \pi}e^{-\left(\frac{\delta(t)}{2\sqrt t}\right)^2}\frac{\sqrt \varepsilon}{\sqrt t}\, s\right]. \tag{74}$$

In the asymptotic limit, the second term in the argument of erf can be considered small, so a Taylor expansion was used to get the last equation. In order to match to the boundary layer solution of eqn. 73 we must have

$$1 - \alpha\,\mathrm{erf}\left(\frac{\delta(t)}{2\sqrt t}\right) = -\frac{\partial T}{\partial s}\Big|_{s=0}\sqrt{\frac{\pi}{2}}$$

$$\Longrightarrow \alpha\,\mathrm{erf}\left(\frac{\delta(t)}{2\sqrt t}\right) = 1 + \frac{\partial T}{\partial s}\Big|_{s=0}\sqrt{\frac{\pi}{2}}, \tag{75}$$

which demands

$$\delta(t) = 2\beta\sqrt{t} \; ; \; \beta \text{ constant,} \qquad (76)$$

$$\alpha = \frac{1 + \frac{\partial T}{\partial s}\Big|_{s=0}\sqrt{\frac{\pi}{2}}}{\text{erf}\,\beta}. \qquad (77)$$

Then the outer expansion in the asymptotic limit is

$$T_0^o \simeq \frac{1 + \frac{\partial T}{\partial s}\Big|_{s=0}\sqrt{\frac{\pi}{2}}}{\sqrt{\pi}} \frac{e^{-\beta^2}}{\text{erf}\,\beta} \frac{\sqrt{\varepsilon}}{\sqrt{t}}\, s - \frac{\partial T}{\partial s}\Big|_{s=0}\sqrt{\frac{\pi}{2}}. \qquad (78)$$

In order to match this with the inner solution the coefficient multiplying s should be $O(\varepsilon^0)$. Taking $\beta = \gamma\sqrt{\varepsilon}$, where $\gamma \sim O(10^0)$ is a numerical constant, accomplishes this, and leads to

$$T_0^o \simeq \frac{1 + \frac{\partial T}{\partial s}\Big|_{s=0}\sqrt{\frac{\pi}{2}}}{2\gamma\sqrt{t}}\, s - \frac{\partial T}{\partial s}\Big|_{s=0}\sqrt{\frac{\pi}{2}} \qquad (79)$$

in the asymptotic limit. This pins down the (scaled) liquid/solid boundary position

$$\delta(t) = 2\gamma\sqrt{\varepsilon t}. \qquad (80)$$

Matching then demands

$$\frac{\partial T}{\partial s}\Big|_{s=0}\left[1 + \sqrt{\frac{\pi}{2}}\right] = \frac{1 + \frac{\partial T}{\partial s}\Big|_{s=0}\sqrt{\frac{\pi}{2}}}{2\gamma\sqrt{t}}, \qquad (81)$$

which gives

$$\frac{\partial T}{\partial s}\Big|_{s=0} = \frac{1}{\sqrt{2t}\left(1 + \sqrt{\frac{\pi}{2}}\right) - \sqrt{\frac{\pi}{2}}}, \qquad (82)$$

a remarkably simple result, which indicates that the temperature gradient at $s = 0$ decays algebraically. The constant $\gamma \sim O(10^0)$ was assigned as $\gamma = \frac{1}{\sqrt{2}}$ to facilitate comparison with the Stefan model.

In summary, as a result of matching at leading order, we find

$$T_0^o(x,t) = 1 - \frac{x}{\delta(t)} - \frac{\partial T}{\partial s}\Big|_{s=0}\sqrt{\frac{\pi}{2}}\frac{x}{\delta(t)}$$

$$= 1 - \frac{x}{\delta(t)} - \frac{\sqrt{\frac{\pi}{2}}}{\sqrt{2t}\left(1 + \sqrt{\frac{\pi}{2}}\right) - \sqrt{\frac{\pi}{2}}}\frac{x}{\delta(t)}, \qquad (83)$$

$$\phi_0^o(x,t) = 1, \qquad (84)$$

and

$$T_0^i(s,t) \simeq \frac{\partial T}{\partial s}\Big|_{s=0}\left[s + \sqrt{\frac{\pi}{2}}\,(s-1)\,H(s-1)\right]$$

$$\simeq \frac{1}{\sqrt{2t}\left(1 + \sqrt{\frac{\pi}{2}}\right) - \sqrt{\frac{\pi}{2}}}\left[s + \sqrt{\frac{\pi}{2}}\,(s-1)\,H(s-1)\right], \qquad (85)$$

$$\phi_0^i(s,t) \simeq 1 - e^{-\frac{s^2}{2} - Bs}, \qquad (86)$$

where we have presumed that $B = \frac{\partial \phi}{\partial s}\Big|_{s=0}$ is sufficiently small that

$$\cosh B \simeq 1 \; ; \; \text{erfc}\,\frac{1}{\sqrt{2}}B \simeq 1 \; ; \; \Omega = e^{\frac{1}{2}B^2} \simeq 1.$$

Note that the last equation, for $\phi_0^i(s,t)$ demands the term involving B (no matter how small) to provide a good description for the true behavior of $\phi(s,t)$ at leading order in the boundary layer for small s. Note also that a psuedo-steady form for $T_0^o(x,t)$ arises naturally since transient terms $\sim \delta'(t) = \sqrt{\frac{\varepsilon}{2t}}$ were neglected in formulating boundary layer equations. In other words, the presumption $\sqrt{\frac{\varepsilon}{2t}} << \sqrt{\varepsilon} \Rightarrow \sqrt{2t} >> 1$ is built into the calculation, and this is the requirement for a psuedo steady solution for $T_0^o(x,t)$.

A.4 Comparison with Stefan model

This section provides the details of the comparison presented in section 3.3. The (dimensional) Stefan model is

$$\frac{\partial}{\partial t}T = \alpha\frac{\partial^2}{\partial x^2}T \quad \text{for } 0 < x < \Delta(t); \qquad (87)$$

$$T(x, t = 0) = T_m \quad \text{for } 0 < x < \Delta(t),$$

$$T(x = 0, t) = T_0 < T_m \quad \text{for } t > 0; \qquad (88)$$

$$k\frac{\partial}{\partial x}T\Big|_{x=\Delta(t)} = \rho\hat{L}\phi_m\frac{d}{dt}\Delta. \qquad (89)$$

Extra conditions willl lead to $\Delta(t)$:

$$T(x = \Delta(t), t) = T_m \; ; \; \Delta(t = 0) = 0. \qquad (90)$$

Scaling the temperature as was done previously is convenient:

$$\bar{T} = \frac{T_m - T}{T_m - T_o}$$

gives

$$\frac{\partial}{\partial t}\bar{T} = \alpha\frac{\partial^2}{\partial x^2}\bar{T} \quad \text{for } 0 < x < \Delta(t); \qquad (91)$$

$$\bar{T}(x, t = 0) = 0 \quad \text{for } 0 < x < \Delta(t),$$

$$\bar{T}(x = 0, t) = 1 \quad \text{for } t > 0; \qquad (92)$$

$$-\frac{\partial}{\partial x}\bar{T}\Big|_{x=\Delta(t)} = \frac{\rho\hat{L}\phi_m}{k(T_m - T_o)}\frac{d}{dt}\Delta. \qquad (93)$$

The extra conditions are

$$\bar{T}(x = \Delta(t), t) = 0 \; ; \; \Delta(t = 0) = 0. \qquad (94)$$

Dimensional analysis of the parameter in the second boundary condition shows

$$\frac{\rho\hat{L}\phi_m}{k(T_m - T_o)} \; [=] \; \frac{E/L^3}{E/TL} = \frac{T}{L^2}.$$

There is, evidently, one dimensionless parameter in the model

$$\frac{\alpha\rho\hat{L}\phi_m}{k(T_m - T_o)} = \frac{\hat{L}\phi_m}{\hat{C}(T_m - T_o)} = \lambda,$$

but *no natural length or time scale*. This points to the similarity solution, which is[8]

$$\bar{T} = 1 - \frac{\operatorname{erf}\eta}{\operatorname{erf}\gamma} \; ; \; \eta = \frac{x}{2\sqrt{\alpha t}}; \quad (95)$$

$$\lambda = \frac{e^{-\gamma^2}}{\sqrt{\pi}\gamma\operatorname{erf}\gamma}; \quad (96)$$

$$\Delta(t) = 2\gamma\sqrt{\alpha t}, \quad (97)$$

where γ is the constant determined by the second equation.

From the diffusion equation we see that a psuedo steady solution is valid when

$$\frac{1}{t} << \frac{\alpha}{\Delta^2} \Rightarrow t >> \frac{\Delta^2}{\alpha}.$$

But Δ and t are related via

$$\frac{1}{\Delta} \sim \frac{\rho\hat{L}\phi_m}{k(T_m - T_o)} \frac{\Delta}{t}$$

$$\Rightarrow \Delta^2 \sim \frac{k(T_m - T_o)}{\rho\hat{L}\phi_m}t,$$

so that the first condition can be cast

$$t >> \frac{\Delta^2}{\alpha} \sim \frac{k(T_m - T_o)}{\alpha\rho\hat{L}\phi_m}t$$

$$\Rightarrow \lambda >> 1, \quad (98)$$

which is one condition needed for the boundary layer solution of the crystallisation model. Under these conditions the equation defining γ can be simplified. First note

$$\lambda = \frac{e^{-\gamma^2}}{\sqrt{\pi}\gamma\operatorname{erf}\gamma} \Rightarrow \sqrt{\pi}\gamma\operatorname{erf}\gamma e^{\gamma^2} = \frac{1}{\lambda} << 1,$$

which indicates $\gamma << 1$ when $\lambda >> 1$ so that $e^{\gamma^2} \simeq 1$ and $\operatorname{erf}\gamma \simeq \frac{2}{\sqrt{\pi}}\gamma$ leading to

$$\sqrt{\pi}\gamma\operatorname{erf}\gamma e^{\gamma^2} \simeq 2\gamma^2 = \frac{1}{\lambda} \Rightarrow \gamma \simeq \sqrt{\frac{1}{2\lambda}} = \sqrt{\frac{\varepsilon}{2}}. \quad (99)$$

Under these circumstances the domain on η obeys

$$0 \le \eta \le \frac{x}{2\sqrt{\alpha t}} = \frac{2\gamma\sqrt{\alpha t}}{2\sqrt{\alpha t}} \simeq \sqrt{\frac{\varepsilon}{2}} << 1, \quad (100)$$

so that the Stefan similarity solution simplifies to

$$\bar{T} = 1 - \frac{\operatorname{erf}\eta}{\operatorname{erf}\gamma} \simeq 1 - \frac{\frac{2}{\sqrt{\pi}}\frac{x}{2\sqrt{\alpha t}}}{\frac{2}{\sqrt{\pi}}\gamma} = 1 - \frac{x}{2\gamma\sqrt{\alpha t}} = 1 - \frac{x}{\Delta(t)} = 1 - \frac{\bar{x}}{\delta}, \quad (101)$$

where the last equation results from scaling the numerator and the denominator by the length scale d defined before in section 2.2. The result indicates that the psuedo steady solution for temperature in the Stefan model is nearly identical to the leading order approximation in the crystallisation boundary layer model (note for the latter $\lambda >> 1$ is required for the boundary layer approximation, while a second condition $(2\bar{t})^{1/2} >> 1$ is needed to find simple boundary layer solutions, tantamount to a psuedo-steady approximation for the crystallisation model).

Now we show that the Stefan model solution for $\Delta(t)$ when $\lambda >> 1$ (psuedo steady limit) matches that at leading order from the crystallisation model in the same limit. When $\lambda >> 1$, eqns. 87 and 89 yield

$$\Delta(t) = 2\gamma\sqrt{\alpha t} \simeq \sqrt{2\varepsilon\alpha t}. \quad (102)$$

Now recall the scales used:

$$\bar{t} = \frac{t}{\tau} \; ; \; \tau = \left(R\frac{T_m - T_o}{\phi_m T_m}\right)^{-1} \; ; \; \bar{x} = \frac{x}{d} \; ; d = \sqrt{\frac{\alpha}{R\frac{T_m - T_o}{\phi_m T_m}}} \,,$$

dividing the last equation by d leads to

$$\frac{\Delta}{d} = \delta \simeq \frac{\sqrt{2\varepsilon\alpha t}}{\sqrt{\frac{\alpha}{R\frac{T_m - T_o}{\phi_m T_m}}}} = \sqrt{2\varepsilon\bar{t}}, \quad (103)$$

Which matches the result from the boundary layer model, eqn. 33.